ACS APPLIED MATERIALS & INTERFACES

Research Article

Cite This: ACS Appl. Mater. Interfaces 2018, 10, 16169−16176

www.acsami.org

Chemiresistive Graphene Sensors for Ammonia Detection

Charles Mackin,*[,†] Vera Schroeder,[‡] Amaia Zurutuza,[§] Cong Su,[†] Jing Kong,[†] Timothy M. Swager,*[,‡] and Tomás Palacios*[,†]

[†]Department of Electrical Engineering and Computer Science, Massachusetts Institute of Technology, 77 Massachusetts Avenue, Cambridge Massachusetts 02139, United States

[‡]Department of Chemistry, Massachusetts Institute of Technology, 77 Massachusetts Avenue, Cambridge Massachusetts 02139, United States

[§]Graphenea Headquarters, Paseo Mikeletegi 83, 20009 San Sebastián, Spain

Supporting Information

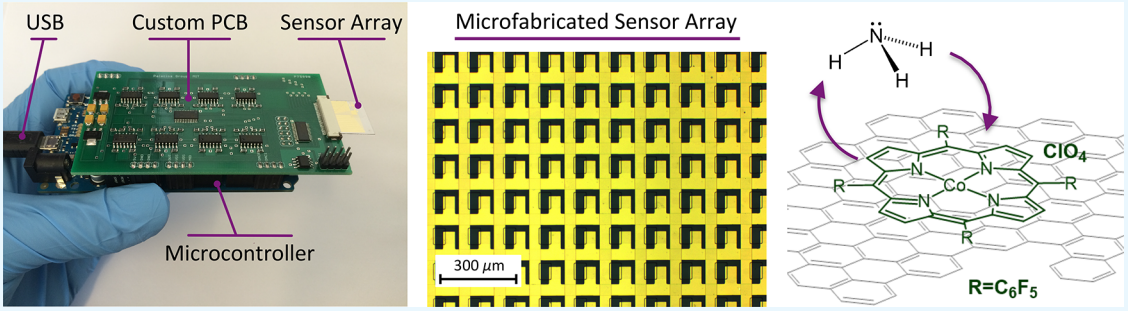

ABSTRACT: The primary objective of this work is to demonstrate a novel sensor system as a convenient vehicle for scaled-up repeatability and the kinetic analysis of a pixelated testbed. This work presents a sensor system capable of measuring hundreds of functionalized graphene sensors in a rapid and convenient fashion. The sensor system makes use of a novel array architecture requiring only one sensor per pixel and no selector transistor. The sensor system is employed specifically for the evaluation of $Co(tpfpp)ClO_4$ functionalization of graphene sensors for the detection of ammonia as an extension of previous work. $Co(tpfpp)ClO_4$ treated graphene sensors were found to provide 4-fold increased ammonia sensitivity over pristine graphene sensors. Sensors were also found to exhibit excellent selectivity over interfering compounds such as water and common organic solvents. The ability to monitor a large sensor array with 160 pixels provides insights into performance variations and reproducibility—critical factors in the development of practical sensor systems. All sensors exhibit the same linearly related responses with variations in response exhibiting Gaussian distributions, a key finding for variation modeling and quality engineering purposes. The mean correlation coefficient between sensor responses was found to be 0.999 indicating highly consistent sensor responses and excellent reproducibility of $Co(tpfpp)ClO_4$ functionalization. A detailed kinetic model is developed to describe sensor response profiles. The model consists of two adsorption mechanisms—one reversible and one irreversible—and is shown capable of fitting experimental data with a mean percent error of 0.01%.

KEYWORDS: *graphene, chemiresistive sensors, porphyrin, $Co(tpfpp)ClO_4$, NH_3 sensors*

1. INTRODUCTION

The primary objective of this work is to demonstrate a novel sensor system as a convenient vehicle for scaled-up repeatability and the kinetic analysis of a pixelated testbed. This work develops a sensor system capable of measuring hundreds of functionalized graphene sensors in a rapid and convenient fashion. The sensor system makes use of a novel array architecture requiring only one sensor per pixel and no selector transistor. The sensor system is employed specifically for the evaluation of $Co(tpfpp)ClO_4$ functionalization of graphene sensors for the detection of ammonia as an extension of previous work.

Graphene is a two-dimensional carbon allotrope consisting of an atomically thin layer of sp^2-bondeds carbon atoms arranged in a hexagonal lattice structure.[1−4] Key material properties include high carrier mobilities,[5] low optical absorption,[6,7] mechanical strength and flexibility,[6−10] and chemical stability.[11−14] Excellent chemical stability is critical for the direct interface with the chemical environments without the need for protective coatings.[11,13−16] These material properties, in combination with the emergence of scalable graphene production,[17,18] have led to extensive interest in graphene-based gas sensors.[19−21] Specifically, ultrasensitive gas sensors are possible wherein the entire active channel is capable of interacting with the analyte with potential for added features such as flexibility and transparency.

Received: January 16, 2018
Accepted: April 11, 2018
Published: April 11, 2018

DOI: 10.1021/acsami.8b00853
ACS Appl. Mater. Interfaces 2018, 10, 16169−16176

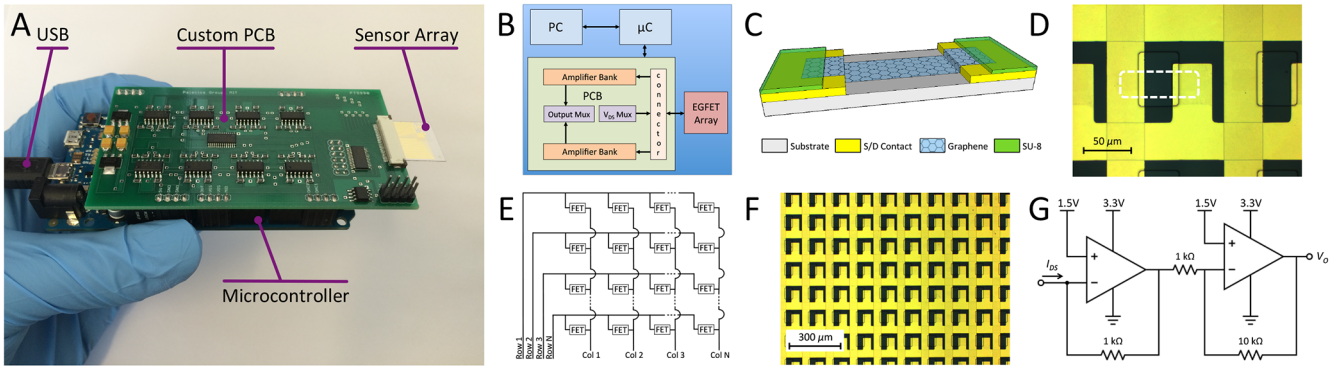

Figure 1. (A) Complete measurement system and sensor array insert, (B) system overview, (C) graphene sensor diagram, (D) microscope image of graphene sensor with channel region outlined in white (dashed), (E) sensor array architecture, (F) microscope image of graphene sensor array, and (G) transimpedance amplifier schematic.

Conductivity-based detection of ammonia has been reported for metal-oxide based sensors,[22−24] conductive polymer-based sensors,[25−28] as well as conductive polymer sensors functionalized with metal-complexes.[29] Additionally, graphene-based chemiresistive sensors have been shown to provide suitable platforms for the detection of ammonia in the gas phase.[30−33] Seredych et al.[34,35] demonstrated the adsorption of ammonia on pristine graphene oxide and determined the interactions to be the result of ammonia reacting with surface groups on the graphene oxide. Conductivity-based ammonia detection with graphene has been reported for pristine,[36,37] polyaniline-functionalized,[30,38,39] SnO_2 and CuO nanostructure decorated,[32] Cu-based MOF/graphene hybridized,[40] fluorinated,[41] and NO_2-doped[31] graphene sensors.

Recently, we demonstrated the sensitive and selective detection of amines via noncovalent functionalization of carbon nanotubes (CNTs) with cobalt *meso*-arylporphyrins.[42] Herein, we apply a similar modular functionalization scheme to an array of microfabricated graphene-based sensors. Porphyrins are particularly well-matched to graphene sensors because they provide excellent sensitivity while producing minimal perturbation to graphene's band structure and electrical properties. Specifically, metalloporphyrins form noncovalent interactions with the graphene leaving the π-bonds responsible for graphene's unique electrical properties intact.[43] Many metalloporphyrins exhibit strong dipoles when bound to analyte and relatively weak dipoles in their unbound states.[44] This is particularly true for cobalt porphyrin when bound to NH_3.[45] These strong dipole interactions serve to alter the carrier concentration in the underlying graphene and ultimately modulate sensor conductivity based on analyte concentration.[44,46] Porphyrins also represent an attractive means of functionalization because they provide a high degree of selectivity.[46,47]

The graphene sensor array is designed as an insertable chip for use in conjunction with a custom readout system. The readout system was designed to be compact and include universal serial bus (USB) connectivity for portability and ease of use. It also includes custom data acquisition software. The combination of these features enables high-quality data acquisition for hundreds of sensors in a rapid and convenient fashion. In previous works, sample sizes and analysis were extremely limited—ranging from individual devices to tens of devices at best.[42,43] The ability to monitor large sample sizes (N = 160) provides new insights into performance variation and reproducibility. The data available from the fabricated sensor array was also used to develop a detailed kinetic model describing sensor response profiles to changing ammonia concentrations. Measurements of the adsorption kinetics of ammonia on graphene films are limited and have been previously determined only for graphene decorated with platinum nanoparticles.[48]

2. EXPERIMENTAL SECTION

2.1. Sensor Array Fabrication. Graphene chemiresistive sensors consist of a functionalized graphene channel between two conductive source-drain contacts. Fabrication of an array of sensors begins with clean glass substrate on which a two-layer metal grid is microfabricated to provide access lines to individual sensors. Commercial-grade graphene is transferred over the array and etched to define the graphene channel regions for each pixel. A passivation layer is deposited on top of the sensor array in which windows are opened to expose the graphene channel region of each pixel.

The graphene sensor array is designed as an insertable chip. The array takes advantage of wire sharing to the extent possible and enables access to M x N sensors using only M + N wires, where M and N represent the number of rows and columns, respectively. Source-drain current signals from the graphene sensors are amplified and converted to voltages using custom-designed circuitry that is packaged into a small form factor printed circuit board (PCB). The custom-PCB is further interfaced with a microcontroller, which enables sensor readout using an analog-to-digital converter (ADC) and data transmission to a personal computer for data recording and analysis. An overview of the graphene sensor system and its key components is presented in Figure 1A−G. Detailed information regarding sensor array fabrication and readout system design is included in the Supporting Information.

2.2. Sensor Array Functionalization. 5,10,15,20-Tetrakis-(pentafluorophenyl)porphyrinatocobalt(III) perchlorate—also referred to as cobalt porphyrin and Co(tpfpp)ClO_4—is depicted in Figure 2 and was synthesized according to previously published procedures.[42] After synthesis, the porphyrin compound was dissolved in dichloromethane (DCM) at a concentration of 0.075 mg/mL. The

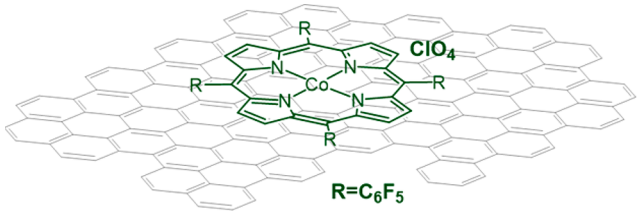

Figure 2. Chemical structure of the Co(tpfpp)ClO_4 selector unit on top of a graphene sheet.

DOI: 10.1021/acsami.8b00853
ACS Appl. Mater. Interfaces 2018, 10, 16169−16176

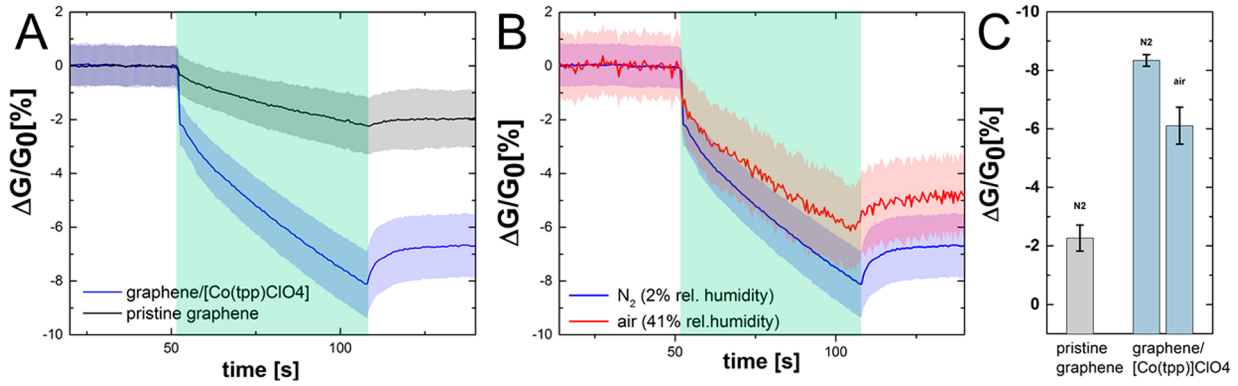

Figure 3. Percentile change in conductance of graphene sensor at an applied voltage of 100 mV. (A) Mean change in conductance upon exposure to 160 ppm of NH_3 in nitrogen of the pristine graphene sensor and the Co(tpfpp)ClO_4 functionalized graphene sheet with shaded regions representing plus or minus one standard deviation from the mean. (B) Mean change in conductance of the Co(tpfpp)ClO_4 functionalized graphene sheet upon exposure to 160 ppm of NH_3 in dry nitrogen and air with 41% relative humidity. Shaded regions represent plus or minus one standard deviation from the mean. Green highlighted regions represent time under ammonia exposure. (C) Percentile change in conductance upon exposure to 160 ppm of NH_3 for 60 s.

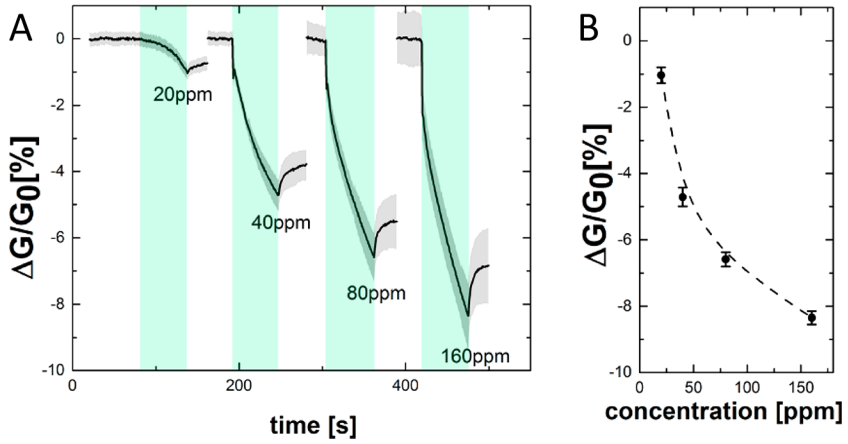

Figure 4. (A) Mean percent change in conductance of functionalized graphene sensors in response to four different concentrations of NH_3. Shaded regions represent plus or minus one standard deviation from the mean. The green highlighted region represents the time under ammonia exposure. (B) Mean sensor response as a function of NH_3 concentration for a fixed exposure time of 60 s.

sensor array was functionalized with one microliter of the porphyrin solution, which was dropcast on the array and allowed to air-dry. Further details regarding sensor array functionalization are provided in the Supporting Information.

3. RESULTS AND DISCUSSION

3.1. Control Comparisons. Initial investigations quantify the sensor responses to changing concentrations of ammonia. Sensor array fabrication, functionalization, and detection methods are all detailed in the Supporting Information. Figure 3A shows the average change of conductance normalized to the initial conductance of the sensor. The response of all sensors—functionalized and unfunctionalized—in this study is semi-dosimetric. The sensor array comprised of pristine graphene shows moderate response toward 160 ppm ammonia ($-2.27 \pm 0.44\%$ $\Delta G/G_0$). As an all-surface material, graphene's electrical properties are highly sensitive to surface molecular interactions, which alter graphene's carrier concentration and resulting conductivity. Ammonia possesses a dipole moment of 1.42 D. As a result, pristine graphene is expected to exhibit some innate sensitivity to ammonia concentration as well as other environmental factors.[16,21] Our findings are consistent with previous results in which ammonia was found to reduce graphene conductivity through competition with the p-doping effect of physisorbed oxygen.[20]

The ammonia response is found to increase 4-fold upon graphene functionalization with Co porphyrin ($-8.34 \pm 0.19\%$). This is comparable to previously reported conductivity-based sensors.[32,36,40−42] The robustness of the sensor when operated under ambient conditions was investigated. Figure 3B reveals that the responsiveness to 160 ppm ammonia decreases slightly from $-8.34 \pm 0.19\%$ to $-6.11 \pm 0.63\%$ when the carrier gas is changed from dry nitrogen to air with 41% relative humidity. All experimental results were obtained at a room temperature of 24 °C. These results confirm sensor functionality in ambient conditions and quantify resilience in the presence of humidity. Homogeneity in responses is shown by $\pm \sigma$ shaded regions and error bars in Figure 3A−C. This attests to the overall reproducibility of the constructed sensors, which includes the microfabrication process and functionalization.

3.2. Sensitivity. Sensor sensitivity was evaluated through investigation of the relationship between NH_3 concentration and the magnitude of the response. Figure 4A shows the mean responses plus or minus one standard deviation for exposures to 20, 40, 80, and 160 ppm of NH_3 in nitrogen. The signal

DOI: 10.1021/acsami.8b00853
ACS Appl. Mater. Interfaces 2018, 10, 16169−16176

strength was found to increase with ammonia concentration (Figure 4B), allowing for quantitative measurement of NH_3 in the experimental window of concentration. The nonlinearity of relationship between ammonia concentration and sensor response is postulated to result from interface reaction kinetics and, more specifically, the reduction in available functionalization binding sites with increased ammonia concentration. This trait is examined in further detail with the development of a kinetics-based sensor response model.

3.3. Selectivity. Selectivity of the functionalized sensors was evaluated through exposure of the sensor array chip to water and a number of volatile organic compounds (VOCs). Figure 5

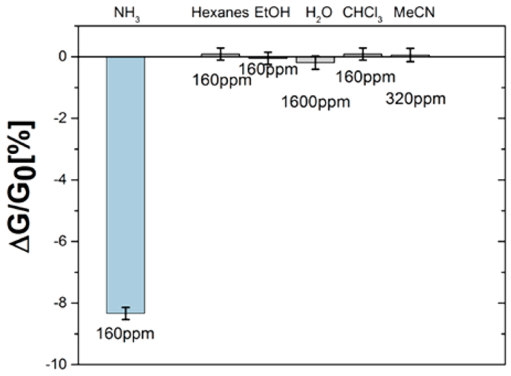

Figure 5. Selectivity comparison of the $Co(tpfpp)ClO_4$ functionalized graphene. Graphene sensors exhibit strong sensitivity to ammonia and suppressed responses to water and other VOCs.

depicts the mean sensor response to ammonia (160 ppm) versus the mean sensor response to hexane (160 ppm), ethanol (160 ppm), water (1600 ppm), chloroform (160 ppm), and acetonitrile (320 ppm). Similar to our reported CNT-based sensing devices,[42] the graphene sensor exhibits negligible sensing responses for water and the examined VOCs (−0.19 to 0.06%) when compared to ammonia (−8.23 ± 0.19%). Thus, the sensitive and selective functionalization originally developed for CNTs effectively translates to graphene-based sensing devices.

3.4. Sensor Kinetics and Modeling. This section develops a quantitative model describing the observed behavior of the sensors in response to changing ammonia concentrations. The observed response curves indicate the existence of two different adsorption mechanisms: one reversible and one irreversible. The presence of an irreversible mechanism is supported by the sensor's failure to return to its initial baseline in the absence of ammonia. The existence of a reversible mechanism is supported by the partial recovery toward the baseline in the absence of ammonia. These two adsorption mechanisms are present in the data depicted in Figure 6A. The irreversible mechanism in the sensor response curves is attributed in part to the incomplete desorption of NH_3 from the Co porphyrin.[42] The reversible mechanism is attributed in part to NH_3 desorption from the Co porphyrin and to weaker reversible effects, such as NH_3 physisorption onto the functionalized graphene surface.

The second-order reversible reaction and kinetic equation are described by eqs 1 and 2, respectively

$$c_R + c_A \underset{\beta}{\overset{\alpha}{\rightleftharpoons}} c_{RA} \tag{1}$$

$$\frac{dc_{RA}(t)}{dt} = \alpha c_R(t)c_A(t) - \beta c_{RA}(t) \tag{2}$$

where α is the rate of the forward reaction, β is the rate of the reverse reaction, c_A is the analyte concentration, c_R is the concentration of reversible binding sites, and c_{RA} is the concentration of analyte bound to reversible binding sites. Similarly, the second-order irreversible reaction and kinetic equation are described by eqs 3 and 4, respectively

$$c_I + c_A \xrightarrow{\gamma} c_{IA} \tag{3}$$

$$\frac{dc_{IA}(t)}{dt} = \gamma c_I(t)c_A(t) \tag{4}$$

where γ is the rate of the forward reaction, c_A is the analyte concentration, c_I is the concentration of irreversible binding sites, and c_{IA} is the concentration of analyte bound to irreversible binding sites. Superimposing the two independent mechanisms and applying initial conditions $c_{RA}(t = 0) = 0$ and $c_{IA}(t = 0) = 0$ along with the fact that $c_A(t)$ is a constant, c_A, produces eq 5

$$c_X(t) = c_{RA}(t) + c_{IA}(t) = \frac{\alpha c_A C_{RT}}{\alpha c_A + \beta}[1 - e^{-(\alpha c_A + \beta)t}] + C_{IT}[1 - e^{-\gamma c_A t}] \tag{5}$$

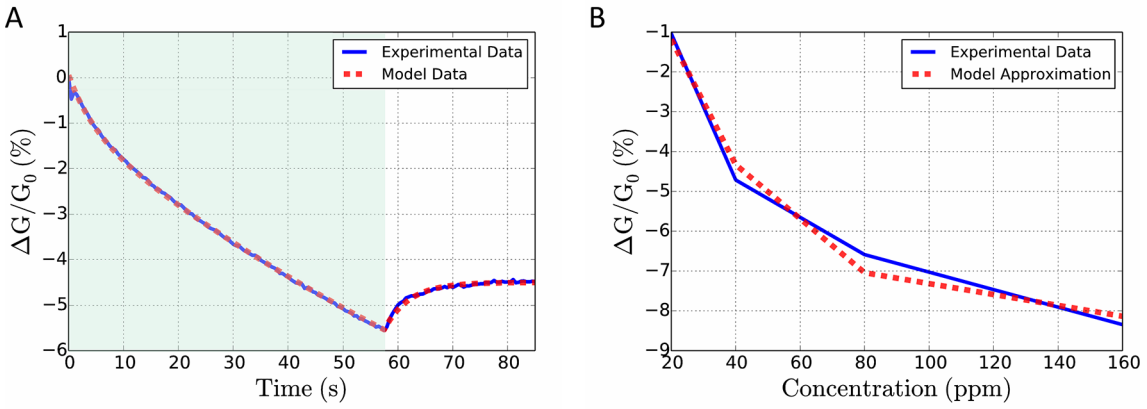

Figure 6. (A) Mean graphene sensor response to 80 ppm of NH_3 exposure and subsequent exposure to pure N_2. Green highlighted region represents time under ammonia exposure. (B) Graphene sensor response for 60s NH_3 exposures as a function of increasing NH_3 concentration.

DOI: 10.1021/acsami.8b00853
ACS Appl. Mater. Interfaces 2018, 10, 16169−16176

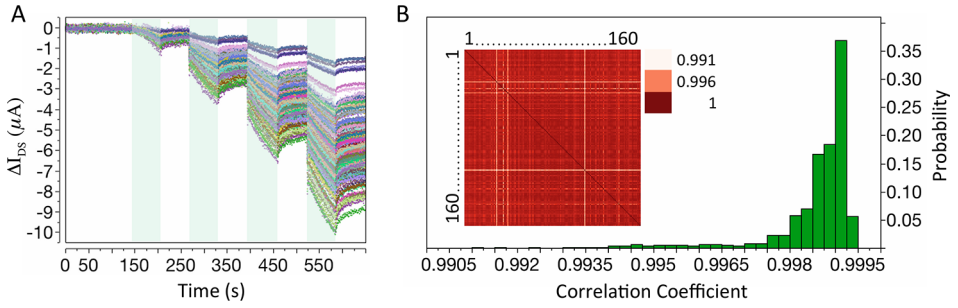

Figure 7. (A) Sensor responses to 20, 40, 80, and 160 ppm of NH_3 with 60-s exposures to pure N_2 occurring at regular intervals. Green highlighted regions represent time under ammonia exposure. Each sensor response is represented by a different color. The legend is omitted due to the large sample size. (B) Probability distribution of correlation coefficients across sample size of N = 160 and corresponding heat map of correlation coefficients (inset) with red and blue indicating correlation coefficients of 1 and −1, respectively.

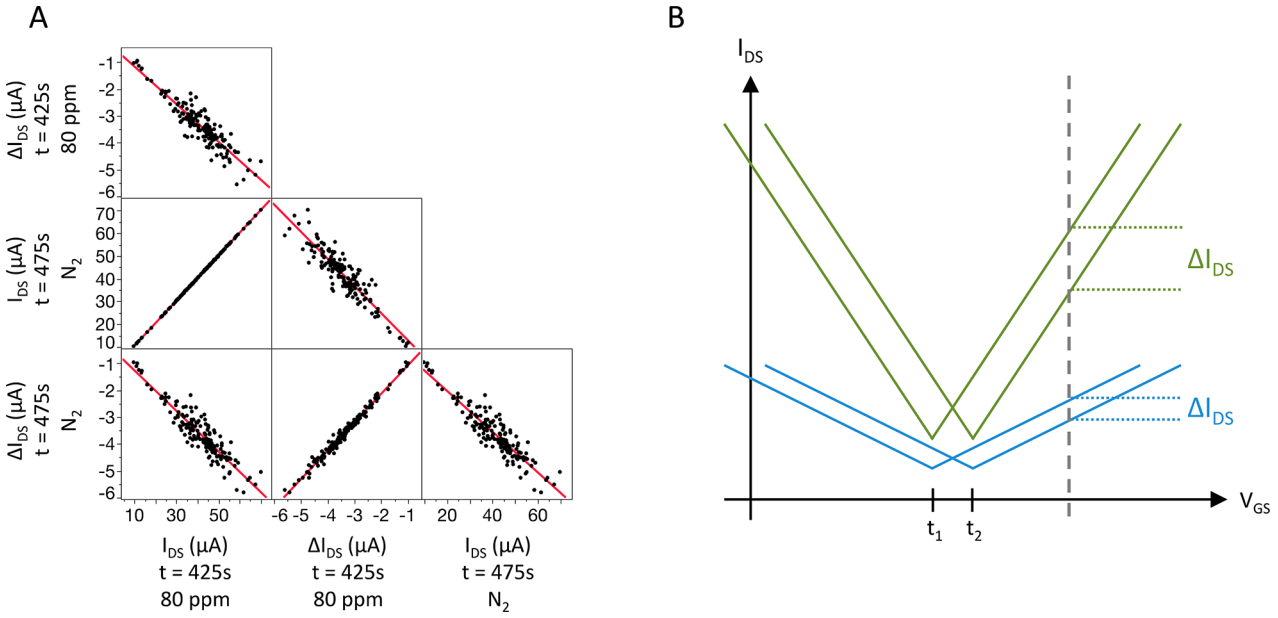

Figure 8. (A) Scatterplot matrix showing relationships between sensor I_{DS} and ΔI_{DS} under different operating conditions (NH_3 vs N_2) and (B) idealized geometric explanation for the observed graphene sensor behavior.

where $c_X(t)$ represents the total doping concentration on the sensor, C_{RT} represents the total number of reversible binding sites, and C_{IT} is the total number of irreversible binding sites. Graphene exhibits a cone-shaped band structure and linear $I-V$ characteristic. The mean of the maximum ΔI_{DS} across the experiment is 6.7 μA whereas the average operating current I_{DS} is 44 μA. Linearity of the graphene $I-V$ characteristic coupled with the small ΔI_{DS} response to changing doping allows the $I-V$ characteristic to be accurately approximated as linear over the small range of interest. See Figure S4. Therefore, doping $c_X(t)$ is proportional to I_{DS}, and by extension $\Delta G/G_0$, leading to eq 6

$$\Delta G/G_0 = H_0 + H_R e^{-(\alpha c_A+\beta)t} + H_I e^{-\gamma c_A t} \quad (6)$$

where H_R is a constant proportional to the number of reversible binding sites, H_I is a constant proportional to the number of irreversible binding sites, and H_0 is a constant accounting for the sensor baseline response. The derived model is fit to the experimental data as shown in Figure 6A. The full sensor response to the presence and absence of analyte is given by a piecewise model detailed in the Supporting Information. The derived piecewise model is shown capable of fitting experimental data exceptionally well resulting in mean percent error of only 0.01%.

The irreversible reaction due to Co(tpfpp)ClO_4 functionalization produces the stronger signal, $H_I > H_R$, as is expected. The reversible reaction, however, reaches equilibrium more quickly indicating a faster time constant. Sensor response for a fixed exposure time of 60 s is found to decay with increasing analyte concentration c_A as shown in Figure 6B. This trend is consistent with the kinetic model given in eq 6.

3.5. Sensor Variation and Reproducibility. The ability to interrogate a large sample size (N = 160) provides new insights into performance variation and reproducibility—two critical factors in the development of practical sensor systems. Correlation coefficients between sensor responses are investigated to assess the overall consistency in response across the sensor array. Correlation coefficients were calculated between every pairwise combination of sensors. The mean correlation coefficient was found to be 0.999. This near perfect linear relationship between sensor responses means variability in responses such as those depicted in Figure 7A are in fact near perfect scalar multiples of each other. This is an important finding because it allows variations in sensitivity to be readily "normalized out" in a noncomputationally expensive fashion

DOI: 10.1021/acsami.8b00853
ACS Appl. Mater. Interfaces 2018, 10, 16169−16176

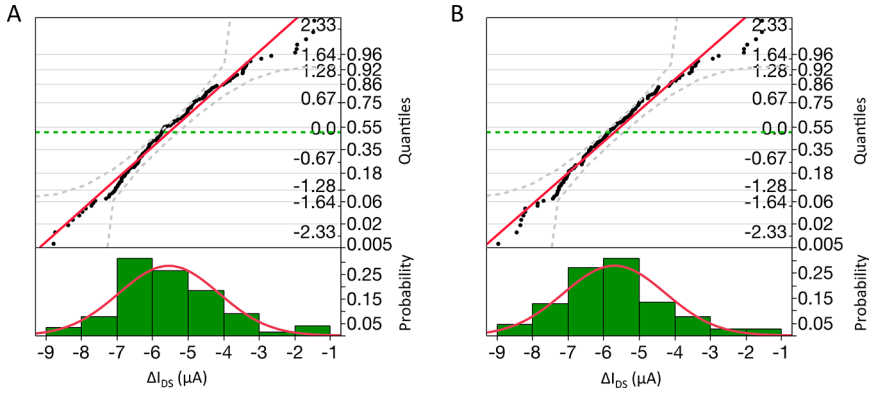

Figure 9. Sensor response distributions and normal quantile plots for (A) sensor exposure to 160 ppm of NH_3 and (B) subsequent exposure to pure N_2.

through multiplication of the sensor array responses by a constant matrix.

No sensor responses were found uncorrelated or inversely correlated—meaning there were no outliers in sensor response. In fact, the minimum correlation coefficient between any two sensors was approximately 0.991. This attests to the consistency of the sensor fabrication process and excellent reproducibility of the Co(tpfpp)ClO_4 functionalization chemistry. *P*-values corresponding to the correlation coefficients were less than 0.0001. The probability distribution for correlation coefficients and corresponding heat map (inset) are provided in Figure 7B.

Further analysis shows that sensors with higher source-drain current I_{DS} also exhibit higher sensitivities ΔI_{DS}. This is shown in Figure 8A by the four plots exhibiting negative regression slopes. The plots compare ΔI_{DS} (sensitivity) versus I_{DS} for different operating conditions (e.g., in the presence of NH_3 and pure N_2.) Regardless of the operating conditions, sensitivity ΔI_{DS} is linearly related to operating current I_{DS}. This finding is consistent with the fact that variation in sensitivity stems from variation in the sensor operating current. This is demonstrated geometrically using idealized graphene $I-V$ curves shown in Figure 8B. Changes in analyte concentration are known to alter the doping of the graphene channel and effectively shift the $I-V$ curve of the graphene sensor. This is a well-established phenomenon for direct current graphene-based sensors and represents the fundamental operating principle for these devices irrespective of application.[16,19,20,49−56] This implies that variation in sensitivity ΔI_{DS} may be minimized by reducing the variation in the underlying sensor operating current I_{DS}. This may be achieved by reducing variation in graphene material properties through the development of more uniform graphene growth, transfer, and microfabrication techniques.

The two plots in Figure 8A with positive regression slopes are comparisons between I_{DS} and ΔI_{DS} for different operating conditions. Sensors exhibiting higher I_{DS} current under one condition (e.g., exposure to NH_3) were found to consistently exhibit higher I_{DS} currents under other conditions (e.g., exposure to pure N_2). In addition, sensors exhibiting the highest sensitivities ΔI_{DS} under one condition continue to exhibit highest sensitivities under other operating conditions. Thus, sensor rank in terms of performance remains consistent despite changes in operating conditions. It is important to note the high degree of linearity in the regression slopes. This supports sensor operation that closely resembles the idealized depiction in Figure 8B. Any nonlinearity in the $I-V$ curve would manifest itself as nonlinearity in the regression slopes.

Sensor response variations are examined for two cases of importance: sensor operation in the presence of NH_3 and sensor operation in the absence of NH_3. More specifically, sensitivity data ΔI_{DS} is examined for 160 ppm of NH_3 exposure (t = 550 s) and for subsequent exposure to pure N_2 (t = 625 s). Figure 9 shows variations exhibit nearly ideal normal distributions under both operating conditions. This allows sensor performance variations to be accurately modeled using Gaussian distributions for quality engineering purposes. This is an important finding because the overall variation in sensitivity encapsulates a number of underlying variations including nonuniformities in the graphene material, the microfabrication process, and application of functionalization chemistry. Normal quantile plots show that sensitivity variations mimic nearly ideal normal distributions with experimental data falling within the 95% confidence limits (gray dashed) and having a 50th percentile (green dashed) close to the sample mean.

5. CONCLUSIONS

This work develops a novel sensor system as a convenient vehicle for scaled-up repeatability and the kinetic analysis of a pixelated testbed. The compact sensor system is capable of monitoring hundreds of graphene sensors in a rapid and convenient fashion. Co(tpfpp)ClO_4 functionalization of graphene sensors was found to increase sensitivity to ammonia 4-fold over pristine graphene sensors. Sensor conductance was found to decay with increasing ammonia concentration, which is consistent with a reduction in the number of available functionalization binding sites for higher concentration exposures. Sensors also possess excellent selectivity with responses to ammonia being orders of magnitude greater than the responses to interfering compounds, such as water and common organic solvents.

A physical model based on absorption kinetics was developed and shown to accurately describe sensor response profiles. The model comprised two adsorption mechanisms—one reversible and one irreversible—and was shown capable of fitting experimental data with a mean percent error of 0.01%. The model is also consistent with the experimental observation of decayed sensor response in response to increasing ammonia concentration.

The ability to monitor hundreds of sensors provided new insights into performance variations and reproducibility. Co(tpfpp)ClO_4 functionalized graphene sensors were shown to exhibit a mean correlation coefficient of 0.999 indicating highly consistent sensor responses and excellent reproducibility

DOI: 10.1021/acsami.8b00853
ACS Appl. Mater. Interfaces 2018, 10, 16169−16176

of the cobalt porphyrin functionalization. A near perfect correlation coefficient indicates that all sensor response profiles are linearly related. This allows variation in sensor performance to be readily normalized in a noncomputationally expensive fashion through multiplication of the sensor array responses by a constant matrix.

Variation in sensitivity was found highly correlated to variation in the baseline current of the sensor I_{DS}. This implies variation in sensitivity may be minimized by reducing variation in sensor operating current I_{DS}. This may be achieved by reducing variation in graphene material properties through the development of more uniform graphene growth, transfer, and microfabrication techniques. Variations in sensitivity were also shown to exhibit nearly ideal Gaussian distributions. This represents an important finding because variation in sensitivity encompasses variations in the graphene material, sensor microfabrication process, and functionalization. This has important implications for variation modeling, quality engineering, and the further advancement of this sensing technology. The combination of these findings mark an important step in the development of new and practical graphene-based chemical sensors for ammonia detection.

■ ASSOCIATED CONTENT

Supporting Information

The Supporting Information is available free of charge on the ACS Publications website at DOI: 10.1021/acsami.8b00853.

Derivation of the sensor response model, sensor response concentration dependence, graphene $I-V$ curve linearity, sensor system fabrication details, and sensor array functionalization (PDF)

■ AUTHOR INFORMATION

Corresponding Authors

*E-mail: cmackin@mit.edu.
*E-mail: tswager@mit.edu.
*E-mail: tpalacios@mit.edu.

ORCID

Charles Mackin: 0000-0001-8413-5583
Vera Schroeder: 0000-0002-6255-4418
Jing Kong: 0000-0003-0551-1208
Timothy M. Swager: 0000-0002-3577-0510
Tomás Palacios: 0000-0002-2190-563X

Funding

ARO-ISN UARC, Graphene-Based FET Biosensor Platform for Screening Food and Water (W911NF-13-D-0001 T.O.9); Triton Systems, Low Cost Repeatable Bio-FET Sensing (TSI-2445-14-103591); AFOSR FATE MURI, FATE: Foldable and Adaptive Two-Dimensional Electronics (FA9550-15-1-0514); Supported (in part) by the Center for Integrated Quantum Materials under NSF grant DMR-1231319; National Science Foundation (DMR-1410718).

Notes

The authors declare no competing financial interest.

■ REFERENCES

(1) Geim, A. K.; Novoselov, K. S. The Rise of Graphene. *Nat. Mater.* **2007**, *6*, 183−191.
(2) Zhu, Y.; Murali, S.; Cai, W.; Li, X.; Suk, J. W.; Potts, J. R.; Ruoff, R. S. Graphene and Graphene Oxide: Synthesis, Properties, and Applications. *Adv. Mater.* **2010**, *22*, 3906−3924.
(3) Castro Neto, A. H.; Guinea, F.; Peres, N. M. R.; Novoselov, K. S.; Geim, A. K. The Electronic Properties of Graphene. *Rev. Mod. Phys.* **2009**, *81*, 109−162.
(4) Soldano, C.; Mahmood, A.; Dujardin, E. Production, Properties and Potential of Graphene. *Carbon* **2010**, *48*, 2127−2150.
(5) Petrone, N.; Dean, C. R.; Meric, I.; van der Zande, A. M.; Huang, P. Y.; Wang, L.; Muller, D.; Shepard, K. L.; Hone, J. Chemical Vapor Deposition-Derived Graphene with Electrical Performance of Exfoliated Graphene. *Nano Lett.* **2012**, *12*, 2751−2756.
(6) Kim, K. S.; Zhao, Y.; Jang, H.; Lee, S. Y.; Kim, J. M.; Kim, K. S.; Ahn, J.-H.; Kim, P.; Choi, J.-Y.; Hong, B. H. Large-Scale Pattern Growth of Graphene Films for Stretchable Transparent Electrodes. *Nature* **2009**, *457*, 706−710.
(7) Bae, S.; Kim, H.; Lee, Y.; Xu, X.; Park, J.-S.; Zheng, Y.; Balakrishnan, J.; Lei, T.; Ri Kim, H.; Song, Y. I.; Kim, Y.-J.; Kim, K. S.; Ozyilmaz, B.; Ahn, J.-H.; Hong, B. H.; Iijima, S. Roll-to-Roll Production of 30-Inch Graphene Films for Transparent Electrodes. *Nat. Nanotechnol.* **2010**, *5*, 574−578.
(8) Stöberl, U.; Wurstbauer, U.; Wegscheider, W.; Weiss, D.; Eroms, J. Morphology and Flexibility of Graphene and Few-Layer Graphene on Various Substrates. *Appl. Phys. Lett.* **2008**, *93*, 051906.
(9) Xu, Y.; Wang, Y.; Liang, J.; Huang, Y.; Ma, Y.; Wan, X.; Chen, Y. A Hybrid Material of Graphene and Poly (3,4-Ethyldioxythiophene) with High Conductivity, Flexibility, and Transparency. *Nano Res.* **2009**, *2*, 343−348.
(10) Lee, C.; Wei, X.; Kysar, J. W.; Hone, J. Measurement of the Elastic Properties and Intrinsic Strength of Monolayer Graphene. *Science* **2008**, *321*, 385−388.
(11) Zhou, M.; Zhai, Y.; Dong, S. Electrochemical Sensing and Biosensing Platform Based on Chemically Reduced Graphene Oxide. *Anal. Chem.* **2009**, *81*, 5603−5613.
(12) Elias, D. C.; Nair, R. R.; Mohiuddin, T. M. G.; Morozov, S. V.; Blake, P.; Halsall, M. P.; Ferrari, A. C.; Boukhvalov, D. W.; Katsnelson, M. I.; Geim, A. K.; Novoselov, K. S. Control of Graphene's Properties by Reversible Hydrogenation: Evidence for Graphane. *Science* **2009**, *323*, 610−613.
(13) Shao, Y.; Wang, J.; Wu, H.; Liu, J.; Aksay, I. A.; Lin, Y. Graphene Based Electrochemical Sensors and Biosensors: A Review. *Electroanalysis* **2010**, *22*, 1027−1036.
(14) Brownson, D. A. C.; Kampouris, D. K.; Banks, C. E. Graphene Electrochemistry: Fundamental Concepts Through to Prominent Applications. *Chem. Soc. Rev.* **2012**, *41*, 6944.
(15) Hess, L. H.; Seifert, M.; Garrido, J. A. Graphene Transistors for Bioelectronics. *Proc. IEEE* **2013**, *101*, 1780−1792.
(16) Dan, Y.; Lu, Y.; Kybert, N. J.; Luo, Z.; Johnson, A. T. C. Intrinsic Response of Graphene Vapor Sensors. *Nano Lett.* **2009**, *9*, 1472−1475.
(17) Li, X.; Cai, W.; An, J.; Kim, S.; Nah, J.; Yang, D.; Piner, R.; Velamakanni, A.; Jung, I.; Tutuc, E.; Banerjee, S. K.; Colombo, L.; Ruoff, R. S. Large-Area Synthesis of High-Quality and Uniform Graphene Films on Copper Foils. *Science* **2009**, *324*, 1312−1314.
(18) Reina, A.; Jia, X.; Ho, J.; Nezich, D.; Son, H.; Bulovic, V.; Dresselhaus, M. S.; Kong, J. Large Area, Few-Layer Graphene Films on Arbitrary Substrates by Chemical Vapor Deposition. *Nano Lett.* **2009**, *9*, 30−35.
(19) Schedin, F.; Geim, A. K.; Morozov, S. V.; Hill, E. W.; Blake, P.; Katsnelson, M. I.; Novoselov, K. S. Detection of Individual Gas Molecules Adsorbed on Graphene. *Nat. Mater.* **2007**, *6*, 652−655.
(20) Gautam, M.; Jayatissa, A. H. Gas Sensing Properties of Graphene Synthesized by Chemical Vapor Deposition. *Mater. Sci. Eng., C* **2011**, *31*, 1405−1411.
(21) Rumyantsev, S.; Liu, G.; Shur, M. S.; Potyrailo, R. A.; Balandin, A. A. Selective Gas Sensing with a Single Pristine Graphene Transistor. *Nano Lett.* **2012**, *12*, 2294−2298.
(22) Wang, G.; Ji, Y.; Huang, X.; Yang, X.; Gouma, P. I.; Dudley, M. Fabrication and Characterization of Polycrystalline WO_3 Nanofibers and Their Application for Ammonia Sensing. *J. Phys. Chem. B* **2006**, *110*, 23777−23782.

DOI: 10.1021/acsami.8b00853
ACS Appl. Mater. Interfaces 2018, 10, 16169−16176

(23) Marquis, B. T.; Vetelino, J. F. A Semiconducting Metal Oxide Sensor Array for the Detection of NO_x and NH_3. *Sens. Actuators, B* **2001**, *77*, 100−110.
(24) Tomchenko, A. A.; Harmer, G. P.; Marquis, B. T.; Allen, J. W. Semiconducting Metal Oxide Sensor Array for the Selective Detection of Combustion Gases. *Sens. Actuators, B* **2003**, *93*, 126−134.
(25) Fiddes, L. K.; Chang, J.; Yan, N. Electrochemical Detection of Biogenic Amines during Food Spoilage Using an Integrated Sensing RFID Tag. *Sens. Actuators, B* **2014**, *202*, 1298−1304.
(26) Tanguy, N. R.; Thompson, M.; Yan, N. A Review on Advances in Application of Polyaniline for Ammonia Detection. *Sens. Actuators, B* **2018**, *257*, 1044−1064.
(27) Hirata, M.; Sun, L. Characteristics of an Organic Semiconductor Polyaniline Film as a Sensor for NH_3 Gas. *Sens. Actuators, A* **1994**, *40*, 159−163.
(28) Kukla, A. L.; Shirshov, Y. M.; Piletsky, S. A. Ammonia Sensors Based on Sensitive Polyaniline Films. *Sens. Actuators, B* **1996**, *37*, 135−140.
(29) Radhakrishnan, S.; Deshpande, S. D. Conducting Polymers Functionalized with Phthalocyanine as Nitrogen Dioxide Sensors. *Sensors* **2002**, *2*, 185−194.
(30) Wu, Z.; Chen, X.; Zhu, S.; Zhou, Z.; Yao, Y.; Quan, W.; Liu, B. Enhanced Sensitivity of Ammonia Sensor Using Graphene/Polyaniline Nanocomposite. *Sens. Actuators, B* **2013**, *178*, 485−493.
(31) Mortazavi Zanjani, S. M.; Sadeghi, M. M.; Holt, M.; Chowdhury, S. F.; Tao, L.; Akinwande, D. Enhanced Sensitivity of Graphene Ammonia Gas Sensors Using Molecular Doping. *Appl. Phys. Lett.* **2016**, *108*, 033106.
(32) Zhang, D.; Liu, J.; Jiang, C.; Liu, A.; Xia, B. Quantitative Detection of Formaldehyde and Ammonia Gas via Metal Oxide-Modified Graphene-Based Sensor Array Combining with Neural Network Model. *Sens. Actuators, B* **2017**, *240*, 55−65.
(33) Ghosh, R.; Midya, A.; Santra, S.; Ray, S. K.; Guha, P. K. Chemically Reduced Graphene Oxide for Ammonia Detection at Room Temperature. *ACS Appl. Mater. Interfaces* **2013**, *5*, 7599−7603.
(34) Seredych, M.; Tamashausky, A. V.; Bandosz, T. J. Graphite Oxides Obtained from Porous Graphite: The Role of Surface Chemistry and Texture in Ammonia Retention at Ambient Conditions. *Adv. Funct. Mater.* **2010**, *20*, 1670−1679.
(35) Seredych, M.; Bandosz, T. J. Combined Role of Water and Surface Chemistry in Reactive Adsorption of Ammonia on Graphite Oxides. *Langmuir* **2010**, *26*, 5491−5498.
(36) Bannov, A. G.; Prášek, J.; Jašek, O.; Zajíčková, L. Investigation of Pristine Graphite Oxide as Room-Temperature Chemiresistive Ammonia Gas Sensing Material. *Sensors* **2017**, *17*, 320.
(37) Wang, Y.; Zhang, L.; Hu, N.; Wang, Y.; Zhang, Y.; Zhou, Z.; Liu, Y.; Shen, S.; Peng, C. Ammonia Gas Sensors Based on Chemically Reduced Graphene Oxide Sheets Self-Assembled on Au Electrodes. *Nanoscale Res. Lett.* **2014**, *9*, 251.
(38) Li, X.; Chen, X.; Yao, Y.; Li, N.; Chen, X. High-Stability Quartz Crystal Microbalance Ammonia Sensor Utilizing Graphene Oxide Isolation Layer. *Sens. Actuators, B* **2014**, *196*, 183−188.
(39) Andre, R. S.; Shimizu, F. M.; Miyazaki, C. M.; Riul, A.; Manzani, D.; Ribeiro, S. J. L.; Oliveira, O. N.; Mattoso, L. H. C.; Correa, D. S. Hybrid Layer-by-Layer (LbL) Films of Polyaniline, Graphene Oxide and Zinc Oxide to Detect Ammonia. *Sens. Actuators, B* **2017**, *238*, 795−801.
(40) Travlou, N. A.; Singh, K.; Rodríguez-Castellón, E.; Bandosz, T. J. Cu−BTC MOF−graphene-Based Hybrid Materials as Low Concentration Ammonia Sensors. *J. Mater. Chem. A* **2015**, *3*, 11417−11429.
(41) Katkov, M. V.; Sysoev, V. I.; Gusel'nikov, A. V.; Asanov, I. P.; Bulusheva, L. G.; Okotrub, A. V. A Backside Fluorine-Functionalized Graphene Layer for Ammonia Detection. *Phys. Chem. Chem. Phys.* **2015**, *17*, 444−450.
(42) Liu, S. F.; Petty, A. R.; Sazama, G. T.; Swager, T. M. Single-Walled Carbon Nanotube/Metalloporphyrin Composites for the Chemiresistive Detection of Amines and Meat Spoilage. *Angew. Chem., Int. Ed.* **2015**, *54*, 6554−6557.
(43) Iezhokin, I.; den Boer, D.; Offermans, P.; Ridene, M.; Elemans, J. A. A. W.; Adriaans, G. P.; Flipse, C. F. J. Porphyrin Molecules Boost the Sensitivity of Epitaxial Graphene for NH_3 Detection. *J. Phys.: Condens. Matter* **2017**, *29*, 065001.
(44) Di Natale, C.; Buchholt, K.; Martinelli, E.; Paolesse, R.; Pomarico, G.; D'Amico, A.; Lundström, I.; Lloyd Spetz, A. Chemical Investigation of Quartz Microbalance and ChemFET Transduction of Molecular Recognition Events in a Metalloporphyrin Film. *Sens. Actuators, B* **2009**, *135*, 560−567.
(45) Cao, Z.; Chen, Q.; Lu, Y.; Liu, H.; Hu, Y. Density Functional Theory Study on the Interaction Between Metalloporphyrins and NH_3. *Int. J. Quantum Chem.* **2013**, *113*, 1137−1146.
(46) Chaudhary, A.; Patra, R.; Rath, S. P. Binding of Catechols to Iron(III)−Octaethylporphyrin: An Experimental and DFT Investigation. *Eur. J. Inorg. Chem.* **2010**, *2010*, 5211−5221.
(47) Auwärter, W.; Écija, D.; Klappenberger, F.; Barth, J. V. Porphyrins at Interfaces. *Nat. Chem.* **2015**, *7*, 105−120.
(48) Gautam, M.; Jayatissa, A. H. Adsorption Kinetics of Ammonia Sensing by Graphene Films Decorated with Platinum Nanoparticles. *J. Appl. Phys.* **2012**, *111*, 094317.
(49) Mackin, C.; Palacios, T. Large-Scale Sensor Systems Based on Graphene Electrolyte-Gated Field-Effect Transistors. *Analyst* **2016**, *141*, 2704−2711.
(50) Mailly-Giacchetti, B.; Hsu, A.; Wang, H.; Vinciguerra, V.; Pappalardo, F.; Occhipinti, L.; Guidetti, E.; Coffa, S.; Kong, J.; Palacios, T. pH Sensing Properties of Graphene Solution-Gated Field-Effect Transistors. *J. Appl. Phys.* **2013**, *114*, 084505.
(51) Ohno, Y.; Maehashi, K.; Yamashiro, Y.; Matsumoto, K. Electrolyte-Gated Graphene Field-Effect Transistors for Detecting pH and Protein Adsorption. *Nano Lett.* **2009**, *9*, 3318−3322.
(52) Hess, L. H.; Jansen, M.; Maybeck, V.; Hauf, M. V.; Seifert, M.; Stutzmann, M.; Sharp, I. D.; Offenhäusser, A.; Garrido, J. A. Graphene Transistor Arrays for Recording Action Potentials from Electrogenic Cells. *Adv. Mater.* **2011**, *23*, 5045−5049.
(53) Kwak, Y. H.; Choi, D. S.; Kim, Y. N.; Kim, H.; Yoon, D. H.; Ahn, S.-S.; Yang, J.-W.; Yang, W. S.; Seo, S. Flexible Glucose Sensor Using CVD-Grown Graphene-Based Field Effect Transistor. *Biosens. Bioelectron.* **2012**, *37*, 82−87.
(54) Lei, N.; Li, P.; Xue, W.; Xu, J. Simple Graphene Chemiresistors as pH Sensors: Fabrication and Characterization. *Meas. Sci. Technol.* **2011**, *22*, 107002.
(55) Ang, P. K.; Chen, W.; Wee, A. T. S.; Loh, K. P. Solution-Gated Epitaxial Graphene as pH Sensor. *J. Am. Chem. Soc.* **2008**, *130*, 14392−14393.
(56) Zhang, M.; Liao, C.; Yao, Y.; Liu, Z.; Gong, F.; Yan, F. High-Performance Dopamine Sensors Based on Whole-Graphene Solution-Gated Transistors. *Adv. Funct. Mater.* **2014**, *24*, 978−985.

DOI: 10.1021/acsami.8b00853
ACS Appl. Mater. Interfaces 2018, 10, 16169−16176